Inorg. Chem. **2006**, *45*, 4007–4015

Effects of Axial Coordination on the Ru–Ru Single Bond in Diruthenium Paddlewheel Complexes

Sanjib K. Patra, Nabanita Sadhukhan, and Jitendra K. Bera*

Department of Chemistry, Indian Institute of Technology, Kanpur 208016, India

Received January 2, 2006

The 1,8-naphthyridine-based (NP-based) ligands with furyl, thiazolyl, pyridyl, and pyrrolyl attachments at the 2-position have been synthesized. Reactions of 3-MeNP (3-methyl-1,8-naphthyridine), fuNP (2-(2-furyl)-1,8-naphthyridine), tzNP (2-(2-thiazolyl)-1,8-naphthyridine), pyNP (2-(2-pyridyl)-1,8-naphthyridine), and prNP^{-1} (2-(2-pyrrolyl)-1,8-naphthyridine) with $[Ru_2(CO)_4(CH_3CN)_6]^{2+}$ lead to $[Ru_2(3\text{-MeNP})_2(CO)_4(OTf)_2]$ (**1**), $[Ru_2(fuNP)_2(CO)_4]_2[BF_4]_2$ (**2**), $[Ru_2(tzNP)_2(CO)_4][ClO_4]_2$ (**3**), $[Ru_2(pyNP)_2(CO)_4][OTf]_2$ (**4**), and $[Ru_2(prNP)_2(CO)_4]$ (**5**). The molecular structures of complexes **1**–**5** have been established by X-ray crystallographic studies. The modulation of the Ru–Ru single-bond distances with axial donors triflates, furyls, thiazolyls, pyridyls, and pyrrolyls has been examined. A small and gradual increase in the Ru–Ru distance is measured with various donors of increasing strengths. The shortest Ru–Ru distance of 2.6071(9) Å is observed for the axially coordinated triflates in complex **1**, and the longest Ru–Ru distance of 2.6969(10) Å is measured for axial pyrrolyls in complex **5**. The Ru–Ru distances in complexes **3** (2.6734(7) Å) and **4** (2.6792(9) Å), having thiazolyls and pyridyls at axial sites respectively, are similar. The Ru–Ru distance for axial furyls in complex **2** (2.6261(9) Å) is significantly shorter than the corresponding distances in **3**, **4**, and **5**. DFT calculations provide insight into the interaction of the Ru–Ru σ orbital with axial donors. The Ru–Ru σ orbital is elevated to a higher energy because of the interaction with axial lone pairs. The degree of destabilization depends on the nature of axial ligands: the stronger the ligand, higher the elevation of Ru–Ru σ orbital. The lengthening of Ru–Ru distances with respect to the axial donors in compounds **1**–**5** follows along the direction pyrrolyl > pyridyl $\approx$ thiazolyl > furyl > triflate, and the trend correlates well with the computed destabilization of the Ru–Ru σ orbitals.

Introduction

The identity of the metal ions, the nature of equatorial ligands, and the closeness of the axial ligands are known to influence the metal−metal separations in paddlewheel complexes. The modulation of metal−metal distances depends on the nature and proximity of the axial ligands provided other factors remain unchanged.[1] Earlier studies had probed the effects of axial coordination on Cr−Cr quadruple bond.[2] Donation of ligand electron density to σ^*/π^* of a Cr−Cr quadruple bond results in significant lengthening of the Cr−Cr distance. Although the effect is less dramatic, weakening of the Rh−Rh single bond resulting from axial coordination has been observed in $[Rh_2]^{4+}$ paddlewheel complexes.[3] We have undertaken a study in which the axial donors in singly bonded $[Ru_2]^{2+}$ complexes are varied, and the changes in Ru−Ru distances are examined.

The 1,8-naphthyridine-based (NP-based) ligands have been employed because of their ability to effectively bridge a dimetal unit.[4] Covalent attachment of an appropriate donor group at the 2-position of NP provides a ligand that bridges the dimetal unit through the N−C−N moiety of the NP fragment and, at the same time, occupies one axial site. One typical example is tzNP (2-(2-thiazolyl)-1,8-naphthyridine)

* To whom correspondence should be addressed. E-mail: jbera@iitk.ac.in.

(1) (a) Cotton, F. A.; Murillo, C. A.; Walton, R. A. *Multiple Bonds Between Metal Atoms*, 3rd ed.; Springer Science and Business Media, Inc.: New York, 2005. (b) Cotton, F. A.; Murillo, C. A.; Walton, R. A. *Multiple Bonds Between Metal Atoms*, 2nd ed.; Clarendon Press: Oxford, U.K., 1993.

(2) (a) Cotton, F. A.; Daniels, L. M.; Murillo, C. A.; Pascual, I.; Zhou, H. C. *J. Am. Chem. Soc.* **1999**, *121*, 6856. (b) Cotton, F. A.; Extine, M. W.; Rice, G. W. *Inorg. Chem.* **1978**, *17*, 176.

(3) (a) Bradley, P. M.; Bursten, B. E.; Turro, C. *Inorg. Chem.* **2001**, *40*, 1376. (b) Cotton, F. A.; Dikarev, E. V.; Petrukhina, M. A.; Stiriba, S.-E. *Inorg. Chem.* **2000**, *39*, 1748. (c) Aullón, G.; Alvarez, S. *Inorg. Chem.* **1993**, *32*, 3712. (d) Clark, R. J. H.; Hempleman, A. J. *Inorg. Chem.* **1989**, *28*, 746. (e) Sowa, T.; Kawamura, T.; Shida, T.; Yonezawa, T. *Inorg. Chem.* **1983**, *22*, 56. (f) Nakatsuji, H.; Ushio, J.; Kanda, K.; Onishi, Y.; Kawamura, T.; Yonezawa, T. *Chem. Phys. Lett.* **1981**, *79*, 299. (g) Cotton, F. A.; Felthouse, T. R. *Inorg. Chem.* **1981**, *20*, 584. (h) Bursten, B. E.; Cotton, F. A. *Inorg. Chem.* **1981**, *20*, 3042. (i) Norman, J. G.; Kolari, H. J. *J. Am. Chem. Soc.* **1978**, *100*, 791. (j) Dubicki, L.; Martin, R. L. *Inorg. Chem.* **1970**, *9*, 673.

10.1021/ic0600073 CCC: $33.50
Published on Web 04/20/2006

Scheme 1

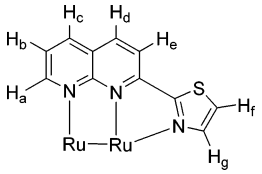

which coordinates to the diruthenium unit as shown in Scheme 1. To explore the dependence of the metal−metal length on axial ligands, the donor units appended at the 2-position of NP are varied. The appendages considered in this work are furyl, thiazolyl, pyridyl, and pyrrolyl groups. The ligands allow us to introduce different donors at sites trans to the Ru−Ru bond. Unlike previous examples,[2,3] the axial donors are not exogenous; rather they are constrained to the NP units. Ligand 3-MeNP (3-methyl-1,8-naphthyridine) has been used, and it is a ligand for which either the solvent molecules or anions are desired to occupy the axial sites.

Although the singly bonded $[Ru_2(CO)_4(CH_3CN)_6][PF_6]_2$ compound was synthesized sometime back,[5] only a few compounds containing $[Ru_2(CO)_4]^{2+}$ are known in the literature.[6] We describe here the compounds obtained by the reaction of 3-MeNP, fuNP (2-(2-furyl)-1,8-naphthyridine), tzNP, pyNP (2-(2-pyridyl)-1,8-naphthyridine), and the anionic form of H-prNP (2-(2-pyrrolyl)-1,8-naphthyridine) with $[Ru_2(CO)_4(CH_3CN)_6]^{2+}$. The variation of Ru−Ru distances with different donors at axial sites is rationalized on the basis of X-ray crystallographic studies and density functional calculations. Spectroscopic and electrochemical properties of the complexes are also reported and described here.

Experimental Section

General Procedure. Materials. All manipulations were carried out under an inert atmosphere with the use of standard Schlenk-line techniques. Glassware was flame-dried under vacuum prior to use. Solvents were dried by conventional methods, distilled over nitrogen, and deoxygenated prior to use.[7] $RuCl_3 \cdot nH_2O$ (39% Ru) was purchased from Arora Matthey, India. The $[Ru_2(CO)_4(CH_3CN)_6][X]_2$ (X = BF_4 or OTf) compounds were synthesized following a procedure similar to that for the synthesis of $[Ru_2(CO)_4(CH_3CN)_6][PF_6]_2$.[5] The ligands 3-MeNP, fuNP, tzNP, pyNP, and H-prNP were prepared by the Friedlander condensation of 2-aminonicotinaldehyde with the corresponding acyl derivatives.[8] Synthetic procedures and NMR data for the ligands are provided as supplementary information.

Physical Measurements. Infrared spectra were recorded in the range of 4000−400 cm^{-1} on a Vertex 70 Bruker spectrophotometer on KBr pellets. ^1H NMR spectra were obtained on a JEOL JNM-LA 400 MHz spectrometer. Electronic absorptions were measured on a Lambda-20 Perkin-Elmer spectrophotometer. Cyclic voltammetric studies were performed on a BAS Epsilon electrochemical workstation in acetonitrile with 0.1 M tetra-*n*-butylammonium hexafluorophosphate ($TBAPF_6$) as the supporting electrolyte. The working electrode was a BAS Pt disk electrode; the reference electrode was Ag/AgCl, and the auxiliary electrode was a Pt wire. The ferrocene/ferrocenium couple occurs at $E_{1/2} = +0.51$ (77) V versus Ag/AgCl under the same experimental conditions.

Theoretical Studies. Calculations were performed using density functional theory (DFT) with Becke's three-parameter hybrid exchange functional[9] and the Lee−Yang−Parr correlation functional (B3LYP).[10] The atomic coordinates of the dicationic units $[Ru_2(CO)_4(L)_2]^{2+}$ (L = 3-MeNP, fuNP, tzNP, pyNP) and $[Ru_2(CO)_4(prNP)_2]$ were taken from the single-crystal X-ray structures. The double-ζ basis set of Hay and Wadt (LanL2DZ) with a small-core (1s2s2p3s3p3d) effective core potential (ECP)[11] was used for Ru. The ligand H, C, N, and O atoms were described using the 6-31G-(d,p) basis sets, and the 6-31G+(2d) basis set was employed for the S atom. All calculations were performed with the Gaussian 03 (G03) suite of programs.[12] Orbital diagrams were generated at isosurface of 0.04 using Gaussview 3.0.[13]

Synthesis. Synthesis of $[Ru_2(3\text{-}MeNP)_2(CO)_4(OTf)_2]$ (1). An acetonitrile solution (10 mL) of 3-MeNP (0.016 g, 0.11 mmol) was added dropwise to an acetonitrile solution (15 mL) of $[Ru_2(CO)_4(MeCN)_6][OTf]_2$ (0.040 g, 0.046 mmol), and the mixture was stirred for 8 h at room temperature. The resulting yellow solution was concentrated under vacuum, and 15 mL of ether was added with stirring to induce precipitation. The solid residue obtained was washed with ether (3 × 5 mL) and dried in a vacuum. Yield: 0.030 g (85%). ^1H NMR (CD_3CN): δ 9.08 (m, 2H), 9.00 (s, 2H), 8.57 (td, 2H), 8.43 (d, 2H), 7.69 (m, 2H), 2.53−2.50 (br, 6H). IR (KBr, cm^{-1}): ν(CO) 2045, 1963; ν(OTf^-) 1260.

(4) (a) Collin, J.-P.; Jouaiti, A.; Sauvage, J.-P.; Kaska, W. C.; McLoughlin, M. A.; Keder, N. L.; Harrison, W. T. A.; Stucky, G. D. *Inorg. Chem.* **1990**, *29*, 2238. (b) Binamira-Soriaga, E.; Keder, N. L.; Kaska, W. C.; McLoughlin, M. A.; Keder, N. L.; Harrison, W. T. A.; Stucky, G. D. *Inorg. Chem.* **1990**, *29*, 2238. (c) Binamira-Soriaga, E.; Keder, N. L.; Kaska, W. C. *Inorg. Chem.* **1990**, *29*, 3167. (d) Thummel, R. P.; Decloitre, Y. *Inorg. Chim. Acta* **1987**, *128*, 245 (e) Thummel, R. P.; Lefoulon, F.; Williamson, D.; Chavan, M. *Inorg. Chem.* **1986**, *25*, 1675. (f) Binamira-Soriaga, E.; Sprouse, S. D.; Watts, R. J.; Kaska, W. C. *Inorg. Chim. Acta* **1984**, *84*, 135. (g) Tikkanen, W. R.; Krüger, C.; Bomben, K. D.; Jolly, W. L.; Kaska, W, C.; Ford, P. C. *Inorg. Chem.* **1984**, *23*, 3633. (h) Baker, A. T.; Tikkanen, W. R.; Kaska, W. C.; Ford, P. C. *Inorg. Chem.* **1984**, *23*, 3254. (i) Tikkanen, W.; Binamira-Soriaga, E.; Kaska, W.; Ford, P. *Inorg. Chem.* **1984**, *23*, 141. (j) Tikkanen, W.; Binamira-Soriaga, E.; Kaska, W.; Ford, P. *Inorg. Chem.* **1983**, *22*, 1147. (k) Tikkanen, W. R.; Binamira-Soriaga, E.; Kaska, W. C.; Ford, P. C. *Inorg. Chem.* **1983**, *22*, 1147. (l) Caluwe, P.; Evens, G. *Macromolecules* **1979**, *12*, 803.

(5) Klemperer, W. J.; Zhong, B. *Inorg. Chem.* **1993**, *32*, 5821.

(6) (a) Schäffler, L.; Müller, B.; Maas, G. *Inorg. Chim. Acta* **2006**, *359*, 970. (b) Cripps, G.; Pellissier, A.; Chardon-Noblat, S.; Deronzier, A.; Haines, R. *J. Organomet. Chem.* **2004**, *689*, 484. (c) Haukka, M.; Da Costa, P.; Luukkanen, S. *Organometallics* **2003**, *22*, 5137. (d) Cabeza, J. A.; del Rio, I.; Riera, V.; Suarez, M.; Alvarez-Rua, C.; Garcia-Granda, S.; Chuang, S. H.; Hwu J. R. *Eur. J. Inorg. Chem.* **2003**, 4159. (e) Deacon, B.; Pearson, P.; Skelton, B. W.; Spiccia, L.; White, A. H. *Acta Crystallogr.* **2003**, *C59*, 537. (f) Luukkanen, S.; Haukka, M.; Laine, O.; Venalainen, T.; Vainiotalo, P.; Pakkanen, T. A. *Inorg. Chim. Acta* **2002**, *332*, 25 (g) Chardon-Noblat, S.; Cripps, G. H.; Deronzier, A.; Field, J. S.; Gouws, S.; Haines, R. J.; Southway, F. *Organometallics* **2001**, *20*, 1668 (h) Kepert, C. M.; Deacon, G. B.; Spiccia, L.; Fallon, G. D.; Skelton, B. W.; White, A. H. *J. Chem. Soc., Dalton Trans.* **2000**, 2867. (i) Xu, L.; Sasaki, Y. *J. Organomet. Chem.* **1999**, *585*, 246. (j) Field, J. S.; Haines, R. J.; Parry, C. J. *J. Chem. Soc., Dalton Trans.* **1997**, 2843. (k) Panneerselvam, K.; Lu, T.-H.; Huang, C.-H.; Tung, S.-F.; Shiu, K.-B. *Acta Crystallogr.* **1997**, *C53*, 1782.

(7) Perrin, D. D.; Armarego, W. L. F.; Perrin, D. R. *Purification of Laboratory Chemicals*, 2nd ed.; Pergamon Press: Elmsford, NY, 1980.

(8) (a) Reddy, K. V.; Mogilaiah, K.; Sreenivasulu, B. *J. Indian Chem. Soc.* **1986**, *63*, 443. (b) Thummel, R. P.; Lefoulon, F.; Cantu, D.; Mahadevan, R. J. *J. Org. Chem.* **1984**, *49*, 2208. (c) Majewicz, T. C.; Caluwe, P. *J. Org. Chem.* **1974**, *39*, 720. (d) Hawes, E. M.; Wibberley, D. G. *J. Chem. Soc.* **1966**, 315.

(9) Parr, R. G.; Yang, W. *Density-Functional Theory of Atoms and Molecules*; Oxford University Press: Oxford, U.K., 1989.

(10) (a) Becke, A. D. *J. Chem. Phys.* **1993**, *98*, 5648. (b) Lee, C.; Yang, W.; Parr, R. G. *Phys. Rev. B* **1998**, *37*, 785.

(11) (a) Hay, P. J.; Wadt, W. R. *J. Chem. Phys.* **1985**, *82*, 270. (b) Wadt, W. R.; Hay, P. J. *J. Chem. Phys.* **1985**, *82*, 284. (c) Hay, P. J.; Wadt, W. R. *J. Chem. Phys.* **1985**, *82*, 299.

Table 1. Crystallographic Data and Refinement Parameters for **1**−**5**

	1·2CHCl$_3$	**2**	**3**	**4**·2C$_6$H$_6$·2CH$_3$CN	**5**·1.5 C$_6$H$_6$
empirical formula	$C_{26}H_{18}Cl_6F_6N_4O_{10}Ru_2S_2$	$C_{28}H_{16}B_2F_8N_4O_6Ru_2$	$C_{26}H_{14}Cl_2N_6O_{12}Ru_2S_2$	$C_{48}H_{36}F_6N_8O_{10}Ru_2S_2$	$C_{37}H_{25}N_6O_4Ru_2$
fw	1139.40	880.21	939.59	1265.11	819.77
cryst syst	orthorhombic	monoclinic	monoclinic	monoclinic	triclinic
space group	*Pccn*	*Cc*	*C*2/*c*	*P*2$_1$/*n*	*P*1
a (Å)	16.810(3)	12.336(3)	24.253(5)	13.902(3)	11.302(2)
b (Å)	13.980(3)	18.350(4)	8.804(5)	25.634(5)	16.654(3)
c (Å)	16.714(3)	13.887(3)	16.993(5)	14.045(3)	17.177(3)
α (deg)					85.69(3)
β (deg)		108.01(3)	124.391(5)	93.05(3)	85.53(3)
γ (deg)					86.10(3)
V (Å^3)	3927.7(14)	2989.7(10)	2994(2)	4998.0(17)	3207.8(11)
Z	4	4	4	4	4
ρ_{calcd} (g cm^{-3})	1.927	1.956	2.084	1.681	1.697
μ (mm^{-1})	1.368	1.112	1.405	0.777	0.994
F(000)	2232	1720	1848	2536	1636
reflns					
collected	21 497	9705	9648	28 757	10 732
independent	4002	6198	3685	10 172	10 732
observed [$I > 2\sigma(I)$]	3624	5827	3480	7141	9111
no. of variables	258	412	226	667	883
GOF	1.172	1.095	1.083	1.049	1.046
final R indices	R1 = 0.0581	R1 = 0.0534	R1 = 0.0324	R1 = 0.0631	R1 = 0.0565
[$I > 2\sigma(I)$][a]	wR2 = 0.1318	wR2 = 0.1128	wR2 = 0.0751	wR2 = 0.1564	wR2 = 0.1418
R indices	R1 = 0.0647	R1 = 0.0574	R1 = 0.0348	R1 = 0.0899	R1 = 0.0666
(all data)[a]	wR2 = 0.1353	wR2 = 0.1150	wR2 = 0.0765	wR2 = 0.1714	wR2 = 0.1488

[a] $R1 = \sum||F_o| - |F_c||/\sum|F_o|$ with $F_o^2 > 2\sigma(F_o^2)$; $wR2 = [\sum w(|F_o^2| - |F_c^2|)^2/\sum|F_o^2|^2]^{1/2}$.

Synthesis of [Ru$_2$(fuNP)$_2$(CO)$_4$][BF$_4$]$_2$ (2). The reaction of [Ru$_2$(CO)$_4$(MeCN)$_6$][BF$_4$]$_2$ (0.058 g, 0.079 mmol) and fuNP (0.033 g, 0.17 mmol) was carried out following a procedure similar to that described in the synthesis of complex **1**. The solid residue obtained was washed with benzene (2 × 5 mL) and dried in a vacuum. Yield: 0.057 g (83%). ^{1}H NMR (CD$_3$CN): δ 9.47 (dd, 2H), 8.15 (dd, 2H), 8.12 (d, 2H), 7.75 (d, 2H), 7.71 (d, 2H), 7.55 (d, 2H), 7.48 (q, 2H), 6.61 (q, 2H). IR (KBr, cm^{-1}): ν(CO) 2043, 1965; ν(BF$_4^-$) 1055.

Synthesis of [Ru$_2$(tzNP)$_2$(CO)$_4$][ClO$_4$]$_2$ (3). The reaction of [Ru$_2$(CO)$_4$(MeCN)$_6$][BF$_4$]$_2$ (0.050 g, 0.076 mmol) and tzNP (0.034 g, 0.16 mmol) was carried out following a procedure similar to that described in the synthesis of complex **1**. The solid residue obtained was washed with benzene (2 × 5 mL), dissolved in acetonitrile and recrystallized over a saturated benzene solution of [*n*-Bu$_4$N][ClO$_4$]. Crystals were collected, washed with copious amount of benzene, and dried in a vacuum. Yield: 0.052 g (82%). ^{1}H NMR (CD$_3$CN): δ 8.78 (d, 2H$_g$), 8.66 (d, 2H$_d$), 8.57 (m, 2H$_a$ and 2H$_c$), 8.51 (d, 2H$_f$), 8.29 (d, 2H$_e$), 7.63 (q, 2H$_b$). IR (KBr, cm^{-1}): ν(CO) 2045, 1970; ν(ClO$_4^-$) 1095, 621.

Synthesis of [Ru$_2$(pyNP)$_2$(CO)$_4$][OTf]$_2$ (4). The reaction of [Ru$_2$(CO)$_4$(MeCN)$_6$][OTf]$_2$ (0.053 g, 0.062 mmol) and pyNP (0.027 g, 0.13 mmol) was carried out following a procedure similar to that described in the synthesis of complex **1**. The resulting wine-colored solution was concentrated under vacuum, and 15 mL of benzene was added with stirring to induce precipitation. The solid residue was washed with benzene (2 × 5 mL) and dried in a vacuum. Yield: 0.51 g (81%). ^{1}H NMR (CD$_3$CN): δ 9.54 (d, 2H), 8.71−8.64 (m, 6H), 8.57 (m, 2H), 8.54 (d, 2H), 8.45 (td, 2H), 8.14 (t, 2H), 7.58 (q, 2H). IR (KBr, cm^{-1}): ν(CO) 2042, 1967; ν(OTf$^-$) 1262.

Synthesis of [Ru$_2$(prNP)$_2$(CO)$_4$] (5). To a THF solution of HprNP (0.027 g, 0.14 mmol), 0.09 mL (0.14 mmol) of 1.6 M *n*-BuLi in hexane was added dropwise at −78 °C. The reaction mixture was allowed to come to room temperature, and a THF solution of [Ru$_2$(CO)$_4$(MeCN)$_6$][OTf]$_2$ (0.054 g, 0.063 mmol) was added to it. The orange solution was stirred for 4 h after which the solvent was evaporated in a vacuum resulting in a bright red solid. It was extracted with 15 mL of benzene and filtered through a Schlenk frit. The filtrate was evaporated giving a red powder, which was then crystallized by layering petroleum ether (60−80 °C) over the benzene solution. Yield: 0.031 g (70%). ^{1}H NMR (CDCl$_3$): δ 8.29 (dd, 2H), 7.71 (m, 4H), 7.51 (d, 2H), 7.40 (d, 2H), 7.01 (d, 2H), 6.94 (td, 2H), 6.56 (dd, 2H). IR (KBr, cm^{-1}): ν(CO) 2045, 1967.

X-ray Data Collection and Refinement. Single-crystal X-ray studies were performed on a CCD Bruker SMART APEX diffractometer equipped with an Oxford Instruments low-temperature attachment. Data were collected at 100(2) K using graphite-monochromated Mo Kα radiation (λ_α = 0.71073 Å). The frames were integrated in the Bruker SAINT software package.[14] The data were corrected for Lorentz and polarization effects, and an absorption correction was applied.[15] The structures were solved and refined with the SHELX suite of programs.[16] The data collection and structure solution details for the individual crystal are provided in the Supporting Information. Hydrogen atoms of the ligands, unless mentioned otherwise, were included in the final stages of the refinement and were refined with a typical riding model. ORTEP-

(12) Frisch, M. J.; Trucks, G. W.; Schlegel, H. B.; Scuseria, G. E.; Robb, M. A.; Cheeseman, J. R.; Montgomery, J. A., Jr.; Vreven, T.; Kudin, K. N.; Burant, J. C.; Millam, J. M.; Iyengar, S. S.; Tomasi, J.; Barone, V.; Mennucci, B.; Cossi, M.; Scalmani, G.; Rega, N.; Petersson, G. A.; Nakatsuji, H.; Hada, M.; Ehara, M.; Toyota, K.; Fukuda, R.; Hasegawa, J.; Ishida, M.; Nakajima, T.; Honda, Y.; Kitao, O.; Nakai, H.; Klene, M.; Li, X.; Knox, J. E.; Hratchian, H. P.; Cross, J. B.; Adamo, C.; Jaramillo, J.; Gomperts, R.; Stratmann, R. E.; Yazyev, O.; Austin, A. J.; Cammi, R.; Pomelli, C.; Ochterski, J. W.; Ayala, P. Y.; Morokuma, K.; Voth, G. A.; Salvador, P.; Dannenberg, J. J.; Zakrzewski, V. G.; Dapprich, S.; Daniels, A. D.; Strain, M. C.; Farkas, O.; Malick, D. K.; Rabuck, A. D.; Raghavachari, K.; Foresman, J. B.; Ortiz, J. V.; Cui, Q.; Baboul, A. G.; Clifford, S.; Cioslowski, J.; Stefanov, B. B.; Liu, G.; Liashenko, A.; Piskorz, P.; Komaromi, I.; Martin, R. L.; Fox, D. J.; Keith, T.; Al-Laham, M. A.; Peng, C. Y.; Nanayakkara, A.; Challacombe, M.; Gill, P. M. W.; Johnson, B.; Chen, W.; Wong, M. W.; Gonzalez, C.; Pople, J. A. *Gaussian 03*; Gaussian, Inc.: Pittsburgh, PA, 2003.
(13) Gaussian Inc.: Pittsburgh, PA, 2003.
(14) *14.SAINT+*, Software for CCD difractometers; Bruker AXS: Madison, WI, 2000.
(15) Sheldrick, G. M. *SADABS, Program for Correction of Area Detector Data*; University of Göttingen: Göttingen, Germany, 1999.
(16) (a) *SHELXTL*, version 6.10; Bruker AXS: Madison, WI, 2000. (b) Sheldrick, G. M. *SHELXS-86* and *SHELXL-97*; University of Göttingen: Göttingen, Germany, 1997.

Scheme 2

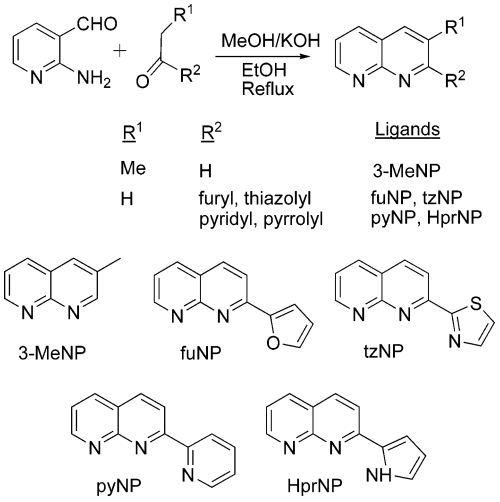

III was used to produce the diagrams.[17] Pertinent crystallographic data for compounds **1**−**5** are summarized in Table 1.

Results and Discussion

Synthesis. The naphthyridine-based ligands were prepared by Friedlander condensation of 2-aminonicotinaldehyde with corresponding acyl derivatives in methanol (Scheme 2).[8] Isolated yields were as high as 80% for all the ligands with the exception of 3-MeNP. Propionaldehyde was used for the synthesis, and a maximum yield of 30% could be achieved after refluxing for 2 days. The ligands were designed to introduce different groups at the axial sites of Ru−Ru single bond. The appendages furyl, thiazolyl, pyridyl, and pyrrolyl were chosen because of their increasing donor strengths.

Reactions of $[Ru_2(CO)_4(CH_3CN)_6][X]_2$ (X = BF_4 or OTf) with 3-MeNP, fuNP, pyNP, and tzNP in acetonitrile and the subsequent crystallization with appropriate anions provide $[Ru_2(3\text{-MeNP})_2(CO)_4(OTf)_2]$ (**1**), $[Ru_2(fuNP)_2(CO)_4][BF_4]_2$ (**2**), $[Ru_2(tzNP)_2(CO)_4][ClO_4]_2$ (**3**), and $[Ru_2(pyNP)_2(CO)_4][OTf]_2$ (**4**). The ligands pyNP and tzNP react instantaneously with the diruthenium precursor; however, the reactions are comparatively slow for 3-MeNP and fuNP. The $prNP^{-1}$ was generated in situ in tetrahydrofuran and was treated with $[Ru_2(CO)_4(CH_3CN)_6][BF_4]_2$ to prepare $[Ru_2(prNP)_2(CO)_4]$ (**5**). Four carbonyl groups bonded to $[Ru_2]^{2+}$ preserve the cis orientation of the ligands and impede metal-based redox reactions.

Isolation of complexes **1**−**5** allowed us to investigate the variation of the Ru−Ru distances with the axial furyl, thiazolyl, pyridyl, and pyrrolyl donors. In the case of 3-MeNP, exogenous triflates occupy the axial sites.

Solid-State Structures. The molecular structure of $[Ru_2(3\text{-MeNP})_2(CO)_4(OTf)_2]$ (**1**) as determined from the X-ray diffraction study is shown in Figure 1. The dinuclear cationic units, $[Ru_2(fuNP)_2(CO)_4]^{2+}$, $[Ru_2(tzNP)_2(CO)_4]^{2+}$, and $[Ru_2(pyNP)_2(CO)_4]^{2+}$, of complexes **2**−**4**, respectively, are depicted in Figures 2−4. Two independent molecules of **5** were located in the asymmetric unit, and slight differences in their metrical parameters were observed. The Ru−Ru distances

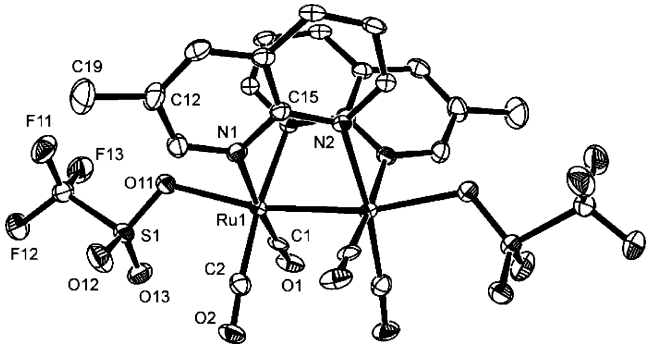

Figure 1. ORTEP diagram of the molecular structure of $[Ru_2(3\text{-MeNP})_2(CO)_4(OTf)_2]$ (**1**) with the important atoms labeled. Hydrogen atoms are omitted for clarity, and the thermal ellipsoids are drawn to 50% probability.

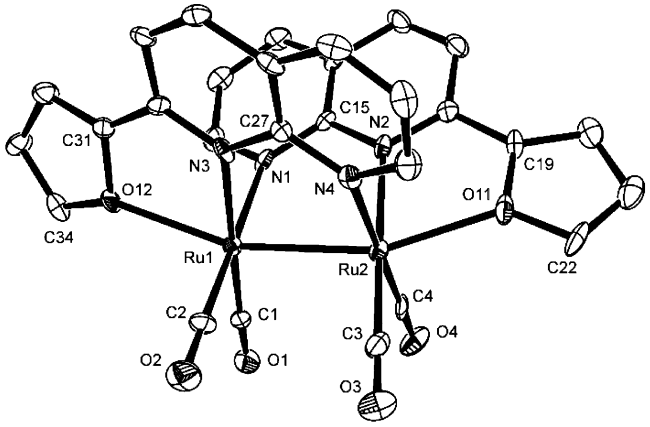

Figure 2. ORTEP diagram of the cationic unit $[Ru_2(fuNP)_2(CO)_4]^{2+}$ in compound **2** with the important atoms labeled. Hydrogen atoms are omitted for clarity and the thermal ellipsoids are drawn to 50% probability.

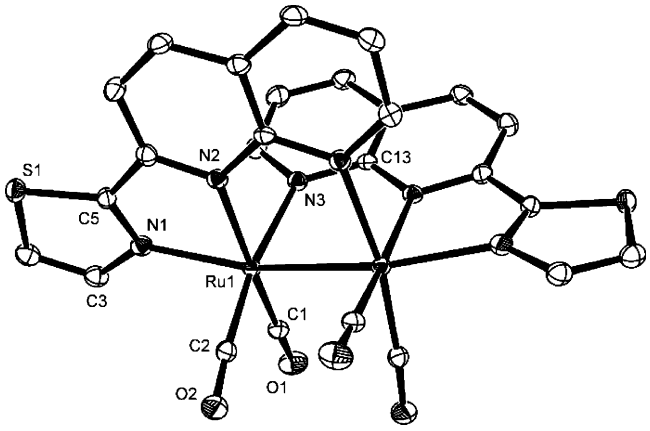

Figure 3. ORTEP diagram of the cationic unit $[Ru_2(tzNP)_2(CO)_4]^{2+}$ in compound **3** with the important atoms labeled. Hydrogen atoms are omitted for clarity and the thermal ellipsoids are drawn to 50% probability.

of the two independent molecules are 2.6969(10) and 2.6949(10) Å. For the purpose of simplicity, we limit our discussion on the molecule that possesses a longer Ru−Ru distance and shorter Ru−N(axial) distances. An ORTEP plot of the $[Ru_2(prNP)_2(CO)_4]$ (**5**) complex is shown in Figure 5, and relevant bond distances and angles are compared in Table 2. The molecular structure of complex **1** consists of a diruthenium unit with two cis 3-MeNP ligands bridging metal centers. Each ruthenium ion is bonded to two cis CO ligands. Molecule **1** has an imposed C_2 axis passing through the center

(17) Farrugia, L. J. *J. Appl. Cryst.* **1997**, *30*, 565.

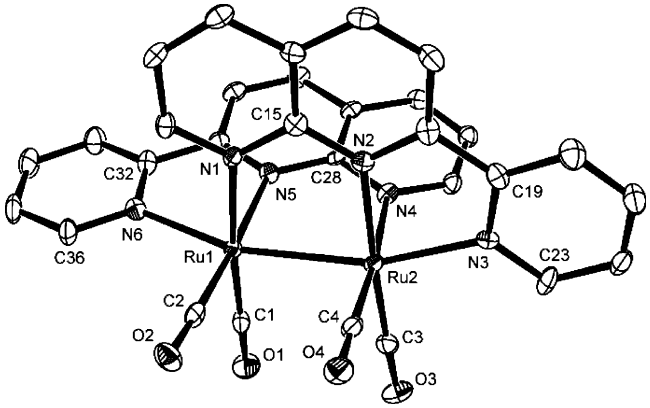

Figure 4. ORTEP diagram of the cationic unit $[Ru_2(pyNP)_2(CO)_4]^{2+}$ in compound **4** with the important atoms labeled. Hydrogen atoms are omitted for clarity, and the thermal ellipsoids are drawn to 50% probability.

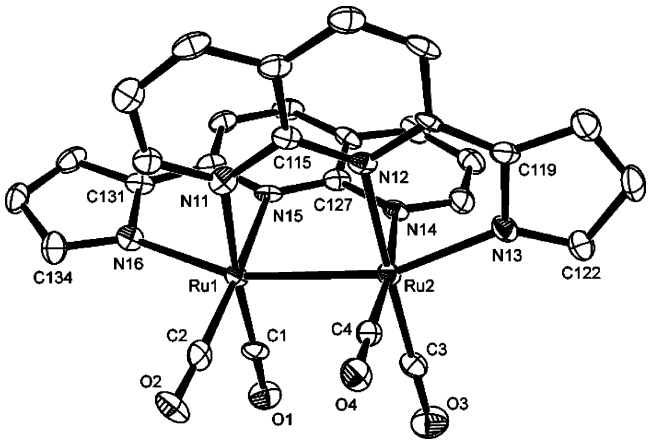

Figure 5. ORTEP diagram of the molecular structure of $[Ru_2(prNP)_2(CO)_4]$ (**5**) with the important atoms labeled. Hydrogen atoms are omitted for clarity, and the thermal ellipsoids are drawn to 50% probability.

of Ru−Ru vector. The significant feature of **1** is that the axial sites are occupied by weakly coordinated triflate anions.

The structure of the cationic part in complex **2** consists of a diruthenium unit spanned by two cis fuNP ligands. The N−C−N unit of the NP fragment bridges two ruthenium centers, and the site trans to Ru−Ru bond is occupied by O atom of furyl appendage. Thus two fuNP ligands occupy four equatorial and two axial positions of the diruthenium unit. Each ruthenium ion is additionally bonded to two cis CO ligands. The molecular structures of complexes **3**−**5** are similar to that of **2**, except that the axial sites are occupied by N atoms of thiazolyl, pyridyl, and pyrrolyl fragments of pyNP, tzNP, and $prNP^{-1}$, respectively. It should be noted here that the N atom of tzNP in complex **3** is coordinated to ruthenium and not S.

The variation of Ru−Ru bond distances in complexes **1**−**5** correlates well with the Ru−L(axial) interactions. A gradual, albeit small, increase in the Ru−Ru distances is measured by varying axial donors of increasing strengths. A plot of the Ru−Ru distances with the donors at axial sites for compounds **1**−**5** is provided in Scheme 3. The longest Ru−Ru distance of 2.6969(10) Å is observed for complex **5** which has pyrrolyl donors at axial sites, and the shortest distance of 2.6071(9) Å is observed for complex **1** in which triflates are coordinated axially. The Ru−Ru distance (2.6261(9) Å) in fuNP complex **2** is 0.019 Å longer than the corresponding distance in **1**. The Ru−Ru distances in complexes **3** (2.6734(7) Å) and **4** (2.6792(9) Å) are similar indicating the comparable donor abilities of the thiazolyl and pyridyl units, respectively. It is also reflected in the close Ru−N(axial) distances. The Ru−Ru distances in **3** and **4** are longer than the corresponding distance in fuNP complex **2** and shorter than the corresponding distance in prNP complex **5**. The shortest Ru−N (axial) distances (2.142(5) Å) in complex **5** go together with the longest Ru−Ru distance reported here.

The Ru−Ru distances are governed by the bridging ligands. A rather long Ru−Ru distance of 2.829(2) Å is reported in unbridged $[Ru_2(bpy)_2(CO)_4(CH_3CN)_2][PF_6]_2$.[6b] The bridging NP ligand constrains the dimetal to a shorter separation than they would otherwise prefer. The longest Ru−Ru distance 2.8731(8) Å is observed in $[Ru_2(CO)_4(CH_3CN)_4(PPh_3)_2][PF_6]_2$ in which PPh_3 ligands are axially bound.[5] The axial interactions of the PPh_3 ligands and the absence of bridging ligands contribute to a long Ru−Ru separation.

The Ru−O (OTf) distances in complex **1** (2.267(4) Å) are shorter than the Ru−O (furyl) distances in **2** (2.294(5) and 2.300(5) Å). The Ru−N(axial) distances in complexes **3**−**5** are in the range of 2.142(5)−2.183(2) Å. The Ru−Ru−O (OTf) angles for unconstrained triflates in complex **1** is 167.50(9)°, and the corresponding Ru−Ru−L(axial) angles in complexes **2**−**5** are in the range of 159.53(13)−162.56(11)°. Near-linear angles suggest a predominant σ interaction of axial donors with the Ru−Ru unit. Carbonyls ligands are eclipsed along the Ru−Ru axis in complex **4** with the C1−Ru1−Ru2−C3 and C2−Ru1−Ru2−C4 torsion angles of 5.3(2) and 4.3(2)°. The corresponding angles in complexes **2** (12.9(3) and 12.1(3)°), **3** (22.77(14)°), and **5** (17.8(3), 19.8(3), 14.3(3), and 13.3(3)°) display deviation from the eclipsed structure. The most staggered orientation of the CO ligands is observed in complex **1** with a C1−Ru1−Ru1−C1 torsion angle of 35.3(2)°.

^{1}H NMR Spectroscopy. The ^{1}H NMR spectroscopy of complex **1** displays five resonances in the aromatic region corresponding to five aromatic protons of 3-MeNP, indicating the equivalence of two 3-MeNP ligands on the NMR time scale. A three-proton signal for the methyl group appears at 2.50−2.53 ppm. Complex **2** shows eight resonances corresponding to eight aromatic protons of fuNP. The proton NMR spectra of compounds **3**, **4**, and **5** exhibit similar patterns with resonances in the aromatic region. The tzNP ligand in complex **3** has seven nonequivalent aromatic protons, and all resonances have been assigned with reasonable certainty (vide supra). The Ha proton, defined in Scheme 1, is positioned above the thiazolyl fragment of the other tzNP, and the resonance is shifted upfield by 0.55 ppm from the corresponding resonance of the free ligand. This is diagnostic of the cis arrangement of the ligands.[19]

Electronic Spectroscopy. The electronic spectra of precursor molecule $[Ru_2(CO)_4(CH_3CN)_6][BF_4]_2$ and compounds **1**−**5** were recorded in acetonitrile in the range of 200−800

(18) Campos-Fernandez, C. S.; Thomson. L. M.; Galan-Mascaros, J. R.; Ouyang, X.; Dunbar, K. R. *Inorg. Chem.* **2002**, *41*, 1523.

Table 2. Relevant Metrical Parameters of Compounds **1**−**5**

	1	**2**	**3**	**4**	**5**
			bond lengths (Å)		
Ru−Ru	2.6071(9)	2.6261(9)	2.6734(7)	2.6792(9)	2.6969(10)
Ru−O(ax)	2.267(4)	2.300(5)			
		2.294(5)			
Ru−N(ax)			2.183(2)	2.171(4)	2.142(5)
				2.179(4)	2.142(5)
Ru−N(eq)	2.178(4)	2.152(6)−2.169(6)	2.154(2)	2.183(4)	2.205(5)
	2.160(4)		2.184(2)	2.136(4)	2.163(5)
				2.135(4)	2.165(5)
				2.190(4)	2.215(5)
Ru−C	1.856(5)	1.856(7)−1.880(8)	1.868(3)	1.846(5)−1.861(5)	1.834(7)−1.866(7)
	1.870(5)		1.860(3)		
C−O	1.146(6)	1.136(9)−1.147(9)	1.135(3)	1.145(6)−1.161(6)	1.142(8)−1.164(8)
	1.139(6)		1.145(3)		
			bond angles (deg)		
Ru−Ru−O(ax)	167.50(9)	159.53(13)			
		159.68(15)			
Ru−Ru−N(ax)			161.63(6)	162.56(11)	159.74(14)
				162.21(10)	159.64(14)
N−Ru−N	85.07(15)	83.3(2)	83.15(9)	85.48(15)	89.40(19)
		86.2(2)		85.32(14)	89.42(18)
C−Ru−N	88.11(18)	92.6(3)−95.4(3)	89.24(11)	91.53(19)−94.15(18)	89.8(2)−92.7(2)
	97.4(2)	176.6(3)−179.0(3)	100.49(11)	175.10(17)−176.36(18)	173.0(2)−177.2(3)
	173.18(18)		170.51(9)		
	173.58(19)		171.29(10)		
C−Ru−C	89.3(2)	88.0(3)	87.68(12)	89.8(2)	87.4(3)
		88.4(3)		88.7(2)	88.6(3)
Ru−C−O	177.8(4)	177.8(7)−178.9(7)	177.5(2)	177.8(4)−179.2(5)	176.2(6)−178.5(6)
	175.1(5)		175.4(2)		
			torsion angles (deg)		
C−Ru−Ru−C	35.3(2)	12.9(3)	22.77(14)	5.3(2)	17.8(3)
		12.1(3)		4.3(2)	19.8(3)
					14.3(3)
					13.3(3)

Scheme 3

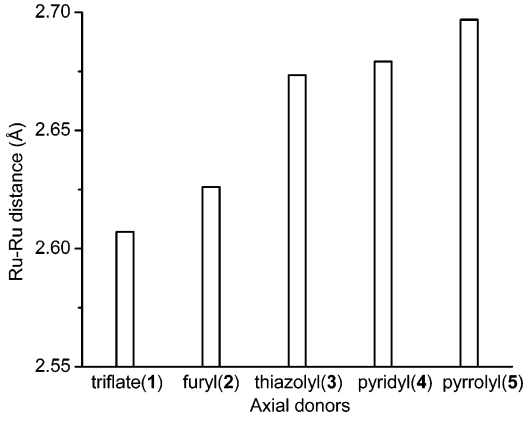

nm. The λ_{max} values with the corresponding ϵ values are given in Table 3. The precursor compound, $[Ru_2(CO)_4(CH_3CN)_6][BF_4]_2$, displays two absorption bands at 275 and 362 nm. The electron configuration of the paddlewheel $[Ru_2]^{2+}$ core is described as $\sigma^2\pi^4\delta^2\delta^{*2}\pi^{*4}$, and likely assignments of the lowest-energy electronic transitions are $\pi^* \rightarrow \sigma^*$ and $\delta^* \rightarrow \sigma^*$.[20] Compound **1** exhibits two absorptions at 301 and 320 nm, the second being a shoulder on the first. Electronic spectra of compounds **2**−**5** exhibit absorptions at higher wavelengths. The lowest-energy λ_{max} was observed for **5**, which has pyrrolyl donors, shown by deep red color of the complex, whereas the other compounds were yellow to orange. The absorption intensities of the compounds were measured to be higher in magnitude than $[Ru_2(CO)_4(CH_3CN)_6][BF_4]_2$ and **1**. This is presumably because of the involvement of greater ligand character in the frontier orbitals of compounds **2**−**5**, and the electronic transitions are likely to be from $[Ru_2]^{2+}$ bond orbitals to empty π^* orbitals, largely, based on the NP ligands.

Table 3. UV−vis Data for $[Ru_2(CO)_4(CH_3CN)_6][BF_4]_2$ and Compounds **1**−**5** in CH_3CN

compound	λ_{max}, nm (log ϵ)			
$[Ru_2(CO)_4(CH_3CN)_6][BF_4]_2$	275 (4.24)	362 (3.56)		
1	301 (4.27)	320 (sh)		
2	263 (4.53)	357 (4.47)	386 (sh)	
3	285 (4.59)	353 (4.64)	368 (sh)	
4	250 (4.54)	276 (4.56)	338 (4.51)	353 (sh)
5	303 (4.47)	448 (4.40)		

Cyclic Voltammetric Studies. The oxidation and reduction potentials of compounds **1**−**5**, as determined by cyclic voltammetry in acetonitrile, are given in Table 4. All the complexes exhibit an irreversible metal-based oxidation. Coordination of two cis 3-MeNP ligands to *cis*-$[Ru_2(CO)_4]^{2+}$ in **1** results into two $1e^-$ irreversible ligand-based reductions at −0.85 and −1.03 V (Figure 6a). Free 3-MeNP undergoes an irreversible $1e^-$ reduction at $E_{pc} = -1.98$ V. The reduction profile of fuNP complex **2** involves four irreversible waves. The cyclic voltammogram of tzNP complex **3** exhibits four

(19) (a) Thummel, R. P.; Lefoulon, F.; Williamson, D.; Chavan, M. *Inorg. Chem.* **1986**, *25*, 1675. (b) Tikkanen, W. R.; Binamira-Soriaga, E.; Kaska, W. C.; Ford, P. C. *Inorg. Chem.* **1984**, *23*, 141.
(20) Martin, D. S., Jr.; Webb, T. R.; Robbins, G. A.; Fanwick, P. E. *Inorg. Chem.* **1979**, *18*, 475.

Table 4. Electrochemical Potentials (V) from Cyclic Voltammetry for Complexes **1**−**5**

compound	oxidation	reduction			
1	1.27[a]	−0.85[b]	−1.03[b]		
2	1.21[a]	−0.75[b]	−0.91[b]	−1.02[b]	−1.15[b]
3	1.34[a]	−0.48 (84)[c]	−0.60 (77)[c]	−1.22 (77)[c]	−1.43 (77)[c]
4	1.30[a]	−0.55 (89)[c]	−0.68 (85)[c]	−1.31 (75)[c]	−1.51 (83)[c]
5	1.29[a]	−1.32[b]	−1.64[b]		

[a] Peak potentials, E_{pa}, for irreversible processes. [b] Peak potentials, E_{pc}, for irreversible processes. [c] Half-wave potentials evaluated from cyclic voltammetry as $E_{1/2} = (E_{pa} + E_{pc})/2$, peak potential differences in mV in parentheses.

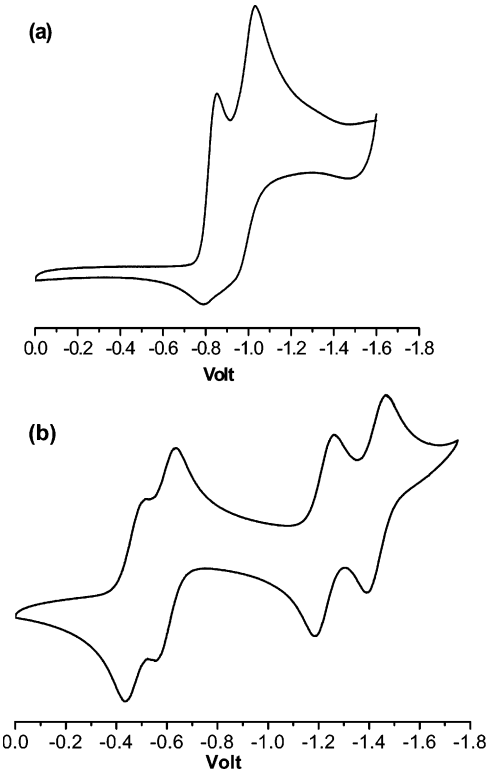

Figure 6. Cyclic voltammograms for (a) **1** and (b) **3** in acetonitrile at a scan rate of 100 mV/s with 0.1 M $[Bu_4N][PF_6]$ as supporting electrolyte.

1e$^-$ reversible reductions at $E_{1/2}(1) = -0.48$ (84) V, $E_{1/2}(2) = -0.60$ (77) V, $E_{1/2}(3) = -1.22$ (77) V, and $E_{1/2}(4) = -1.43$ (77) V (Figure 6b). Similar electrochemical behavior is observed for pyNP complex **4** with reduction potentials located at $E_{1/2}(1) = -0.55$ (89) V, $E_{1/2}(2) = -0.68$ (85) V, $E_{1/2}(3) = -1.31$ (75) V, and $E_{1/2}(4) = -1.51$ (83) V. Complex **5** exhibits two irreversible reduction processes at −1.32 and −1.64 V.

The four reversible waves in complexes **3** and **4** prompted us to look into the ligand-centered reduction processes carefully.[21] The free tzNP and pyNP exhibit two 1e$^-$ reductions: the first reductions are reversible at a potential of $E_{1/2} = -1.49$ (87) and −1.64 (85) V, and the second reductions are irreversible at $E_{pc} = -2.16$ and −2.34 V. Coordination of two ligands to the *cis*-$[Ru_2(CO)_4]^{2+}$ unit

Scheme 4

$$[Ru_2(CO)_4(L3)_2]^{2+} + [Ru_2(CO)_4(L3)_2] \rightleftharpoons 2[Ru_2(CO)_4(L3)_2]^{+}$$

$K_c = 1.05 \times 10^2$ for L3 = tzNP
1.34×10^2 for L3 = pyNP (a)

$$[Ru_2(CO)_4(L3)_2] + [Ru_2(CO)_4(L3)_2]^{2-} \rightleftharpoons 2[Ru_2(CO)_4(L3)_2]^{-}$$

$K_c = 2.92 \times 10^3$ for L3 = tzNP
2.50×10^3 for L3 = pyNP (b)

yields four 1e$^-$ waves indicating electron delocalization in the mixed-valence intermediates (Scheme 4). For complex **3**, the separation between the first two reductions is 120 mV. The comproportionation constant ($K_c(a) = 1.05 \times 10^2$), calculated from the difference of the subsequent reduction potentials, indicates a no-coupling (Class I) to weakly coupled (Class II) system according to the Robin−Day classification.[22] The separation of the $E_{1/2}$ potentials of the third and fourth reductions (210 mV) is found to be larger than the difference of the first and second reduction processes. The $K_c(b)$ obtained is 2.92×10^3, which is in the range of a weakly coupled Class II system. The estimated $K_c(a)$ and $K_c(b)$ values of complex **4** are 1.34×10^2 and 2.50×10^3, indicating that it has an electronic structure comparable to that of complex **3**. The K_c values of fuNP complex **2**, calculated from reduction potentials obtained from the differential pulse voltammetry measurements, are 4.17×10^2 ($K_c(a)$) and 1.70×10^2 ($K_c(b)$), indicating poor electron delocalization in the reduced species.

The estimated K_c values for **3** and **4** are smaller than the corresponding values reported in metal−metal quadruply bonded $[cis\text{-}Mo_2(O_2CCH_3)_2(pyNP)_2]^{2+}$ ($K_c(a) = 1.20 \times 10^4$, $K_c(b) = 2.70 \times 10^5$) or doubly bonded $[Ru_2(O_2CCH_3)_2(pyNP)_2]^{2+}$ ($K_c(a) = 3.90 \times 10^6$, $K_c(b) = 2.70 \times 10^7$).[18] The shorter metal−metal distance does not necessarily lead to higher K_c values. It is our assertion that the ancillary ligands play an important role in the intramolecular ligand-to-ligand charge-transfer process. The Ru−Ru bond orbital, namely, the δ^* orbital, provide a pathway for electron delocalization between the ligand π^* orbitals. Presence of the stronger π-acceptor ligand such as CO reduces the $\pi^*(NP)-\delta^*(Ru_2)-\pi^*(NP)$ overlap and, hence, lowers the K_c values.[23]

Computational Results. To have a better understanding of the interaction of Ru−Ru bond orbitals with axial ligands, closed-shell single-point calculations of dicationic $[Ru_2(3\text{-}MeNP)_2(CO)_4]^{2+}$, $[Ru_2(fuNP)_2(CO)_4]^{2+}$, $[Ru_2(tzNP)_2(CO)_4]^{2+}$, $[Ru_2(pyNP)_2(CO)_4]^{2+}$, and neutral $[Ru_2(prNP)_2(CO)_4]$ were performed using the atomic coordinates provided by the X-ray structures of related compounds. Two axial triflates in **1** are excluded from the calculation. To simplify the discussion, the abbreviations [3-MeNP], [fuNP], [tzNP], [pyNP], and [prNP] are used to designate the species that bears the respective ligands.

Analysis of the calculated orbital occupancies of each species supports the electronic configuration of the $[Ru_2]^{2+}$

(21) (a) Marcaccio, M.; Paolucci, F.; Paradisi, C.; Roffia, S.; Fontanesi, C.; Yellowlees, L. J.; Serroni, S.; Campagna, S.; Denti, G.; Balzani, V. *J. Am. Chem. Soc.* **1999**, *121*, 10081. (b) Krejcik, M.; Vlcek, A. A. *Inorg. Chem.* **1992**, *31*, 2390. (c) Ohsawa, Y.; DeArmond, M. K.; Hanck, K. W.; Morris, D. E. *J. Am. Chem. Soc.* **1983**, *105*, 6522.

(22) (a) Robin, M. B.; Day, P. *Adv. Inorg. Chem. Radiochem.* **1967**, *10*, 247. (b) Kaim, W.; Klein, A.; Glöckle, M. *Acc. Chem. Res.* **2000**, *33*, 755.

(23) (a) Chisholm, M. H. *Dalton. Trans.* **2003**, 3821. (b) Bursten, B. E.; Chisholm, M. H.; Hadad, C. M.; Li, J.; Wilson, P. J. *Chem. Commun.* **2001**, 2382.

Scheme 5

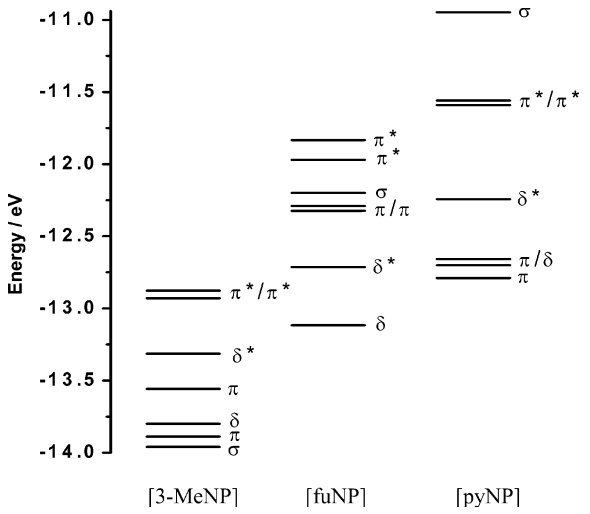

unit as $\sigma^2\pi^4\delta^2\delta^{*2}\pi^{*4}$; this corresponds to a formal Ru−Ru bond order of 1.0. The description of the Ru−Ru bond orbitals as σ, π, and δ is merely a localized description and illustrates the predominant character of the molecular orbitals (MOs). The response of the Ru−Ru bond orbital to axial ligands has been examined. The Ru−Ru σ orbital is elevated in energy because of its interaction with symmetric combination of the axial lone pairs. The shift of Ru−Ru σ bonding electrons to higher energy leads to weakening of Ru−Ru bond: the stronger the axial interaction, the greater the destabilization of the Ru−Ru σ orbital. This is reflected in the relative ordering of the MO levels. The energy levels of the Ru−Ru bond orbitals in [3-MeNP], [fuNP], and [pyNP] are shown in Scheme 5. In [3-MeNP], the lowest-energy metal−metal bond orbital is the Ru−Ru σ orbital. The Ru−Ru σ orbital in [fuNP], as depicted in Figure 7a, is elevated in energy because of the interaction with O lone pairs of the furyl appendages, and it lies below the pair of π^* orbitals (Scheme 5). The extent of destabilization in the case of axial pyridyl donors in [pyNP] is significantly greater resulting in the Ru−Ru σ orbital being the HOMO. Similarly for thiazolyl and pyrrolyl donors in [tzNP] and [prNP], the HOMOs are predominantly Ru−Ru σ-type orbitals. Representative contour surfaces of HOMOs in [pyNP] and [prNP] are shown in Figure 7b and 7c.

The energy levels of the species, as computed from DFT calculations, are found to be shifted. Therefore, the estimation of the degree of destabilization of the Ru−Ru σ orbital rsulting from axial interaction is not straightforward. The difference in energy of the Ru−Ru σ orbital between a particular species and [3-MeNP] was calculated, and it was subtracted from the difference in energy of corresponding δ^* orbitals. The resultant value reflects the degree of axial interaction, taking into consideration that orbitals of δ symmetry are least perturbed by axial ligation. The values calculated for [fuNP], [tzNP], [pyNP], and [prNP] are 25.1, 45.6, 44.8, and 51.3 kcal/mol, respectively, and they illustrate the comparative donor strengths of the appendages. Significantly, the relative destabilization of the Ru−Ru σ orbitals and the lengthening of Ru−Ru distances for different axial donors correlate well. The pyrrolyl donors cause the maximum destabilization of the Ru−Ru σ orbital that is reflected in the longest Ru−Ru distance in complex **5**. Thiazolyl and pyridyl have comparable donor strengths, as indicated by the magnitudes of the elevation of respective Ru−Ru σ orbitals. The result is the small difference (0.006 Å) in the Ru−Ru distances in complexes **3** and **4**. The elevation of Ru−Ru σ orbital in [fuNP] is considerably smaller than that in [tzNP], [pyNP], and [prNP], and it is manifested by a significantly shorter Ru−Ru distance in **2**. The shortest Ru−Ru distance is noted in complex **1** with axial triflates.

It should be pointed out that the axial donation into Ru−Ru π^* orbital contributes to the weakening of the Ru−Ru bond; however, the π effect is minimal because of the near-linear Ru−Ru−L(axial) angles observed in the compounds.[2a]

The weakening of metal−metal and metal−ligand(axial) distances are mutual. The axial ligands weaken the metal−metal bond, and metal−metal bond in turn weakens the metal−ligand(axial) bonds.[24] The axial ligand orbitals interact

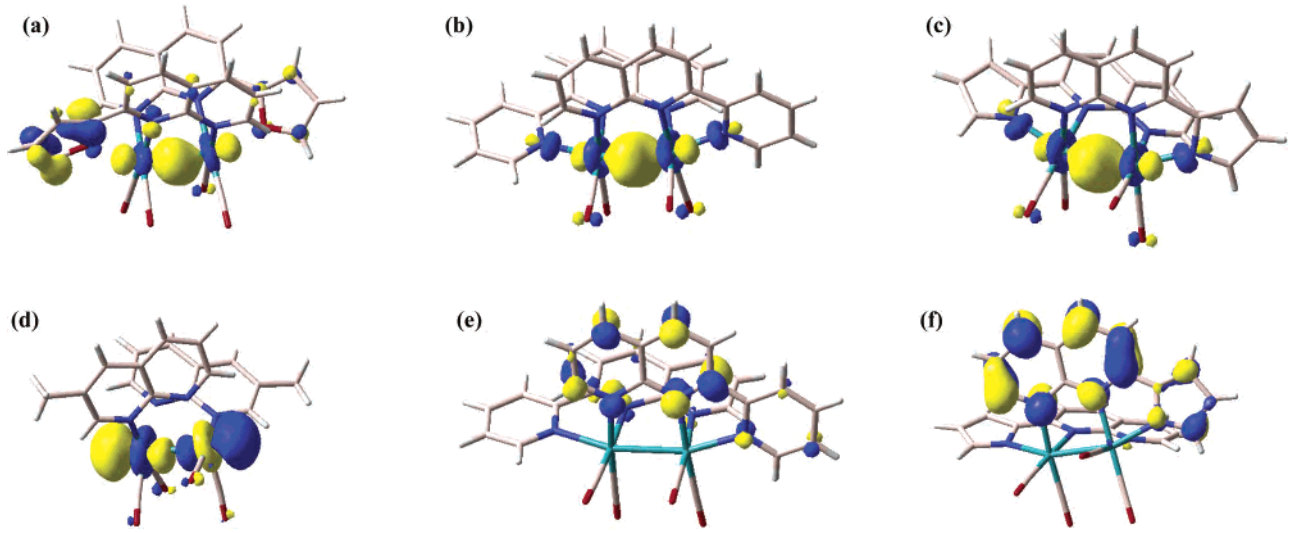

Figure 7. Contour surfaces of (a) the Ru−Ru σ orbital in [fuNP] (HOMO−3), the HOMOs in (b) [pyNP] and (c) [prNP], and the the LUMOs in (d) [3-MeNP], (e) [pyNP], and (f) [prNP].

with the metal−metal bond orbital more weakly than they would if the metal−metal bond was absent.

The LUMO of [3-MeNP] resembles a Ru−Ru σ^* orbital (Figure 7d) and indicates d−d transitions ($\pi^* \rightarrow \sigma^*$ and $\delta^* \rightarrow \sigma^*$) for $[Ru_2(CO)_4(CH_3CN)_6][BF_4]_2$ and **1**. The LUMOs of [fuNP], [tzNP], [pyNP], and [prNP] are primarily ligand π^* orbitals located largely on NP units. Contour diagrams of the LUMOs of [pyNP] and [prNP] are provided in Figure 7e and 7f. The absorptions of **2**−**5** most likely involve MLCT character. Electronic transition from $[Ru_2]^{2+}$ bond orbitals to π^* of NP ligands is in agreement with the high ϵ values observed for the compounds. The maximum destabilization of the Ru−Ru σ orbital in [prNP] leads to smallest HOMO−LUMO gap, exhibiting the lowest-energy λ_{max} for compound **5**.

Summary. In this article, we have examined the response of an Ru−Ru single bond to axial donors. NP-based ligands with furyl, thiazolyl, pyridyl, and pyrrolyl appendages at the 2-position were synthesized. Reactions of fuNP, tzNP, pyNP, and $prNP^{-1}$ with $[cis\text{-}Ru_2(CO)_4(CH_3CN)_6]^{2+}$ provided compounds of the formula $[cis\text{-}Ru_2(CO)_4(L)_2]^{2+/0}$, in which the sites trans to Ru−Ru bond are occupied by the O atoms of furyl or N atoms of thiazolyl, pyridyl, and pyrrolyl attachments. Complex $[Ru_2(3\text{-}MeNP)_2(CO)_4(OTf)_2]$ was synthesized with coordinated triflates at axial sites. X-ray molecular structures of the compounds allowed us to investigate the variation of Ru−Ru distances with axial ligands. A small but gradual increase in the Ru−Ru distances was observed by increasing the donor strength of axial ligands. The shortest Ru−Ru distance was observed for triflates, and the pyrrolyl donors resulted in longest Ru−Ru distance. DFT calculations revealed the destabilizing interaction of Ru−Ru σ orbital with axial lone pairs. The lengthening of Ru−Ru distances with respect to axial donors follows the following trend: pyrrolyl > pyridyl ≈ thiazolyl > furyl > triflate. It also correlates well with the computed destabilization of the Ru−Ru σ orbitals. The lowest-energy transitions and the corresponding extinction coefficients for the compounds are rationalized on the basis of DFT calculations.

Acknowledgment. Authors thank the DST India for support of this research. N.S. thanks C.S.I.R. India for a fellowship.

Supporting Information Available: X-ray crystallographic data for compounds in CIF format, synthesis procedures of the ligands, tables of bond distances and angles for the compounds, NMR and electrochemical data, energy level diagrams, and the surfaces of the MOs. This material is available free of charge via the Internet at http://pubs.acs.org.

IC0600073

(24) Norman, J. G., Jr.; Kolari, H. J. *J. Am. Chem. Soc.* **1978**, *100*, 791.